Remote aerosol species-identification using IR scattering spectroscopy

Shupeng Niu, C. Russell Philbrick, Hans D. Hallen
Physics Department, NC State University, Raleigh, NC 27695-8202

ABSTRACT

Identification of atmospheric aerosol species and their chemical composition may help to trace their source and better estimate their impact on climate and environment. Optical scattering of aerosols depends primarily on aerosol chemical composition, size distribution, particle shape and the wavelength used. Extraction of features due to the aerosol complex refractive index from scattering spectroscopy at a single angle of observation allows composition identification via the spectral fingerprint, as shown computationally with Mie calculations of the optical scattering. Size-dependent scattering effects are eliminated by using near-forward scattering, such as in the scattering aureole. The only features of the aerosol aureole scattering spectra that very rapidly with wavelength are associated with the composition, so the aureole can give a reliable identification of aerosol composition.

Keywords: aerosol scattering, Mie calculation, size distribution, complex refractive index

1. INTRODUCTION

Aerosols are of central importance for atmospheric chemistry and physics, the biosphere, climate, and public health. The airborne solid and liquid particles in the nanometer to several micron size range influence the energy balance of the Earth, the hydrological cycle, atmospheric circulation, and the abundance of greenhouse gases, as well as reactive trace gases. Moreover, they play important roles in the transport of biological organisms and can cause or exacerbate diseases. Atmospheric particles arise from natural sources as well as anthropogenic sources and other human activities. The natural sources include plant emission (plant fragments, microorganisms, pollen, etc.), biomass burning, volcanic activity, desert dust, ocean spray, as well as plant growth in water, and also emissions of particles attributable to the activities of humans arise primarily from burning in industrial processes, automobiles, and fireplaces, nonindustrial sources (e.g. construction work, farming), as well as resuspensions of particles from all of these sources [1-2].

The primary parameters that determine the environmental and health effects of aerosol particles are their chemical composition, concentration, size, and structure. It is most important to determine the composition of aerosols, and thereby, identify the source of the aerosol particles. The composition knowledge is necessary understand their threat to society and develop control strategies [3]. Several methods have been developed to determine the aerosol composition. Most traditional methods for air sampling and chemical analysis of particulate matter are "offline" procedures, and involve the collection of the investigated particles on solid deposition substrates (membrane or fiber filters, inertial impaction plates, thermal or electrostatic precipitation plates) or in a liquid (wetted wall cyclone, impinger, or washing bottle), followed by intermediate steps of sample storage, transport, and preparation, and then a physical or chemical analysis. Several techniques are available for analyzing the composition of collected aerosol particles, such as atomic absorption spectrometry (AAS), x-ray fluorescence analysis (XRF), emission spectrometry (ES), particle-induced x-ray emission (PIXE), scanning electron microscopy (SEM), high performance liquid chromatography (HPLC), gas chromatography (GC), ion chromatography (IC), proton nuclear magnetic resonance (HNMR), secondary ion mass spectrometry (SIMS), inductively coupled plasma mass spectrometry (ICPMS), and laser microprobe mass spectrometry, etc. [4-9]. Some techniques are limited to a single particle at a time, such as scanning electron microscopy [8-9], while most chemical methods analyze large numbers at once. Although methods are generally accurate in describing the material present during analysis, the offline methods are prone to analytical artifacts caused by evaporation of particle components, adsorption or absorption of addition gas-phase components, and chemical reaction during sample collection, storage, transport and preparation. Elaborate sampling techniques are required to minimize these effects, and such sample preparations result in significant costs from special efforts to analyze the samples. Our method does not require sample collection, thereby eliminating several of these shortcomings.

Laser Radar Technology and Applications XIX; and Atmospheric Propagation XI, edited by Monte D. Turner, Gary W. Kamerman, Linda M. Wasiczko Thomas, Earl J. Spillar, Proc. of SPIE Vol. 9080, 908010
 · doi: 10.1117/12.2050689

Real-time measurements of particles are possible with aerosol mass spectrometers. The methods of vaporization, ionization and calibration have improved over the past few years, and aerosol mass spectrometers are able to give reliable quantitative analysis, especially for chemical elements and inorganic species [2,10-12]. Some research groups have also made progress on the identification of biological particles and pathogens [13]. The aerosol mass spectrometer gives reliable analysis, but this equipment also requires sample collection and is quite expensive for in-lab measurements.

The on-line or in-situ methods allow good resolution of spatial and temporal variability of particles. The aethalometer is an instrument that measures the concentration of optically absorbing aerosol particles in real time. The absorption is normally due to black carbon, which is a good tracer for combustion emission. It can also help determine the distributions of absorbing aerosols due to its time resolution capability [14]. Sulfur-specific flame photometer has also been used for the real time measurement of sulfur-containing aerosols by several groups [15-16]. It detects ~394 nm light given off by excited-state S_2 molecules formed when sulfur compounds are burned in a hydrogen-rich flame. These two methods are used for detecting carbon or sulfur-containing aerosols, but both require relative high aerosol densities.

Optical scattering provides significant information about aerosols. Much research has been done to obtain the optical properties of aerosols around the world, and to determine the relationships between optical scattering and the size, shape and chemical composition of the aerosols, by many research groups [17-21]. Multi-static and multi-wavelength light scattering has been used to directly extract aerosol characteristics, including index of refraction, size distribution and number concentration [22]. These optical methods combined with remote sensing techniques, such as Raleigh and Raman Lidar provide important tools to determine the physical and chemical characteristics of aerosols, such as the number density, size, and size distribution. Multi-static lidar, which works at multiple wavelengths and scattering angles, is used to determine the aerosol-species based on their particular optical properties [23-25].

In this paper, we detail a method to determine the complex index of refraction with an optical technique that does not require any knowledge of the particle sizes or distribution. This means that fewer assumptions about particle distributions are required, and the types of efforts mentioned in the previous paragraph are not necessary. The central idea is to create a 'background-free' or 'high frequency' spectral fingerprints can be stored in a library and used to identify an unknown by matching the spectral fingerprint with a measurement that has also had background features, which vary slowly in wavelength, removed. The complex refractive index of aerosols changes with wavelength in a manner that is unique to the material composition of the particle. For most aerosols, the absorption spectrum associated with the imaginary component of the refractive index (or dielectric constant) contains distinctive features at some wavelengths, which provide the fingerprint. We calculated the scattering profiles for a wide range of wavelengths and find similar identifying features despite differences in particle size distribution; thereby demonstrating the opportunity and simplicity for this approach. We have also studied how mixtures can alter some of these strong features, and how they can be corrected using effective medium theory.

2. CALCULATIONS

2.1 Mie Calculations

The code we use is based on that provided by Bohren and Huffman [26], converted to the C-programming language and embedded in a set of driver routines. It uses complex refractive index and size of the particular aerosol as input and calculates the scattering phase function using the scattering matrix elements determined when assuming the incident light is parallel or perpendicular to the scattering plane. The scattering phase function gives the angular distribution of the scattered light. We did the calculations for a range of wavelengths and for several species with different refractive indices; this approach allows us to examine the scattering phase function for the wavelength distribution as a function of angle.

2.2 Choice of aerosols

The aerosols used for Mie calculation were chosen to have the following characteristics: (1) aerosol should be representative of those that exist in the environment, (2) the complex refractive index of these aerosols are available over a broad wavelength range in the literature, (3) the selected aerosols should have spectral features within the wavelength

tuning range of available lasers, and (4) the aerosols should be ones that can be prepared in the laboratory. Aerosols with complex refractive indices features within the visible and infrared region will allow us to investigate the detectability using distinguishing spectral features, as a function of concentration and particle size distribution. This provides the direction for future experimental verification. The chosen materials are: oleic acid, nitric acid trihydrate, sulfuric acid, silica glass, silica type α(crystalline) and ammonium nitrate. Figure 1 shows the complex index of refraction of these materials [27-31]. Note that the primary difference between the sulfuric acid samples with different weight percent is in the magnitude of the indices, and a slight shift in peak wavelength position may also be possible. These effects are quantified using effective medium theory later in the paper.

2.3 Size distribution

Log-normal distributions are used to describe the particle sizes rather than single-sized model [32-34]. The parameters are the number of particles, N, the median diameter, CMD, and mode width, σ_g. For typical Mie scattering, in the infrared range, lognormal distributions with CMD of 10-20 microns are chosen. In order to perform the calculation, we break the size distribution into a series of bins at specific sizes at which the Mie calculations will be performed. The number of particles in each size bin is determined by integration over the distribution, when the total number concentration of particles is assumed to be 2000/cm^3. The result gives us the differential cross section and the inverse scattering length, $K_s = \sigma_1 * N_1 + \sigma_2 * N_2 + \ldots + \sigma_n * N_n$, where σ_1 to σ_n are cross sections for n different size parameters and N_1 to N_n are numbers concentrations of aerosols of these sizes.

3. RESULTS AND DISCUSSION

3.1 Choice of angle for observation

The criterion for choice of angle is selected so that the particle size effects should not be a strong. It is known that the width of the forward scattering lobe of the scattering aureole depends on the particle size and on the wavelength [35], but that the wavelength dependence is relatively weak, so it will only create features that can be removed as a slowly varying background in the measured spectra. Further, the aureole has been shown to be weakly dependent upon particle shape [35]. Finally, the scattering intensity is usually large near the forward scattering direction, so the signal level will be intense within the aureole. These factors suggest that the best angle to use is within the aureole. This section presents the simulations that support this assertion. An angle of 1.8 degrees is chosen for the aureole observation angle. This is large enough that the signal should be separable from the incident beam, yet close enough to the center of the forward lobe that the signal will not be dramatically affected by a change in angle, or integration over a small range of angles by the detector. Calculations for ammonium nitrate aerosols are shown in Fig, 2 for a widely spaced range of angles.

Figure 2(a) and 2(b) show the scattering radiant intensity of ammonium nitrate at different angles, when the particle median diameter is 20 microns. The index of refraction related effects are observed in all cases, although there are other oscillations of similar magnitude at all angles except 1.8 degrees. We observe oscillations in the large angle data, especially at smaller wavelengths, and that complicates the identification of the composition-dependent signals. These oscillations are due to Mie resonances in the scattering by particles, and are expected to be more significant when the size parameter of the particles is close to unity [36]. The wavelength dependence is described through the size parameter $x = 2\pi a/\lambda$. The inverse wavelength dependence also explains the more rapid variation at smaller, rather than larger wavelengths. Despite the stronger features at larger angles, the Mie resonances occupy nearly the same Fourier components as the compositional features, so they cannot be easily separated at angles outside the aureole. We thus are driven to the aureole angles in order to eliminate interference and simplify analysis. Indeed the 1.8-degree data consists of only the spectral features of interest appearing upon a slowly varying background. The calculated intensity associated with the chemical composition also exceeds the other cases by a large amount in this log-scaled graph. The qualitative decrease of the scattering intensity with wavelength at small angles is well known for small particles, and is quartic in the Raleigh regime. The size parameter x is the relevant parameter, so for a fixed particle distribution, scattering decreases with increasing wavelength. At slightly larger angles, this effect would be somewhat ameliorated by the fact that the width of the forward scattering lobe increases as x decreases, but we choose not to make use of it since it would lead to more particle size related background variations. Figure 2(c) shows the calculated spectral fingerprints.

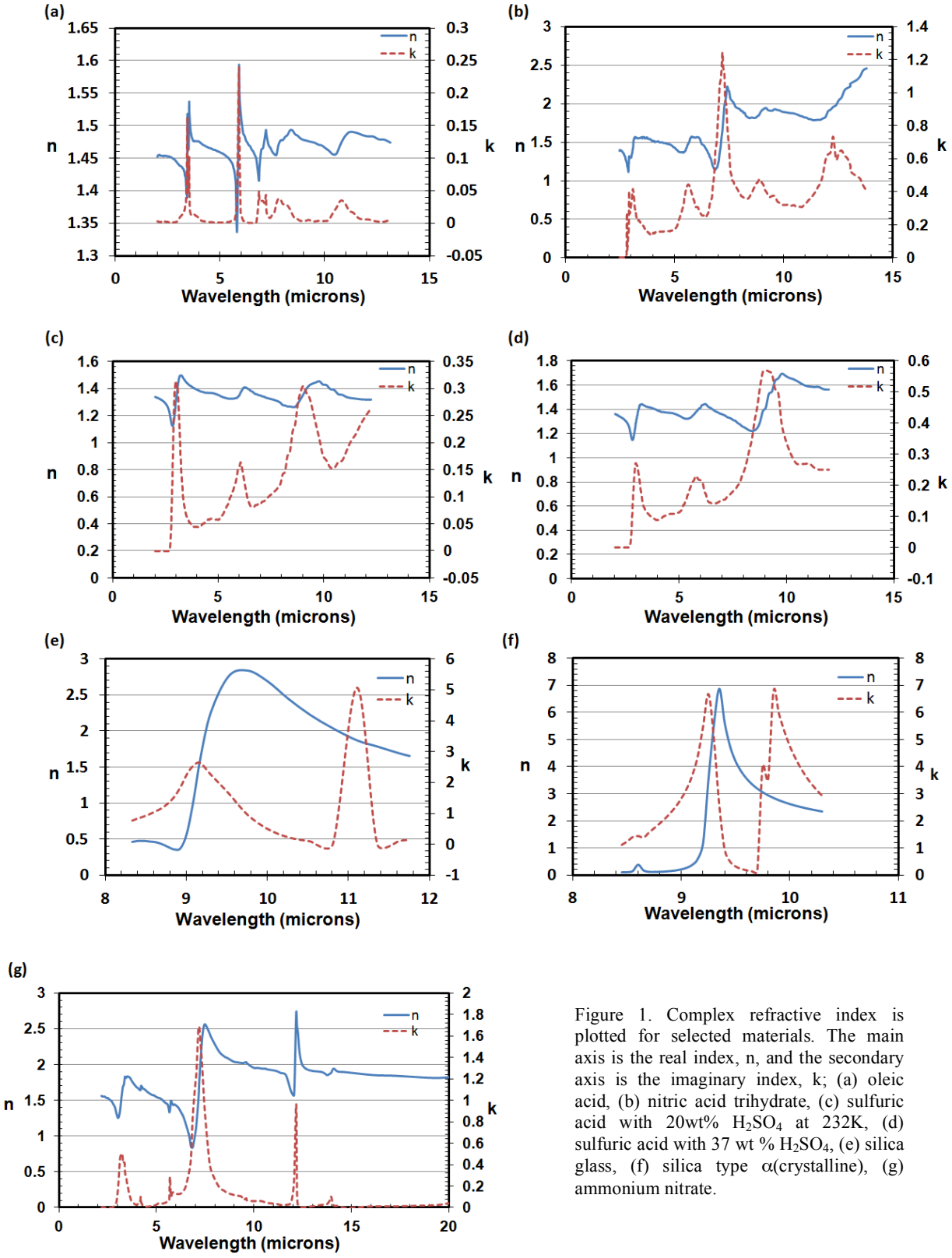

Figure 1. Complex refractive index is plotted for selected materials. The main axis is the real index, n, and the secondary axis is the imaginary index, k; (a) oleic acid, (b) nitric acid trihydrate, (c) sulfuric acid with 20wt% H_2SO_4 at 232K, (d) sulfuric acid with 37 wt % H_2SO_4, (e) silica glass, (f) silica type α(crystalline), (g) ammonium nitrate.

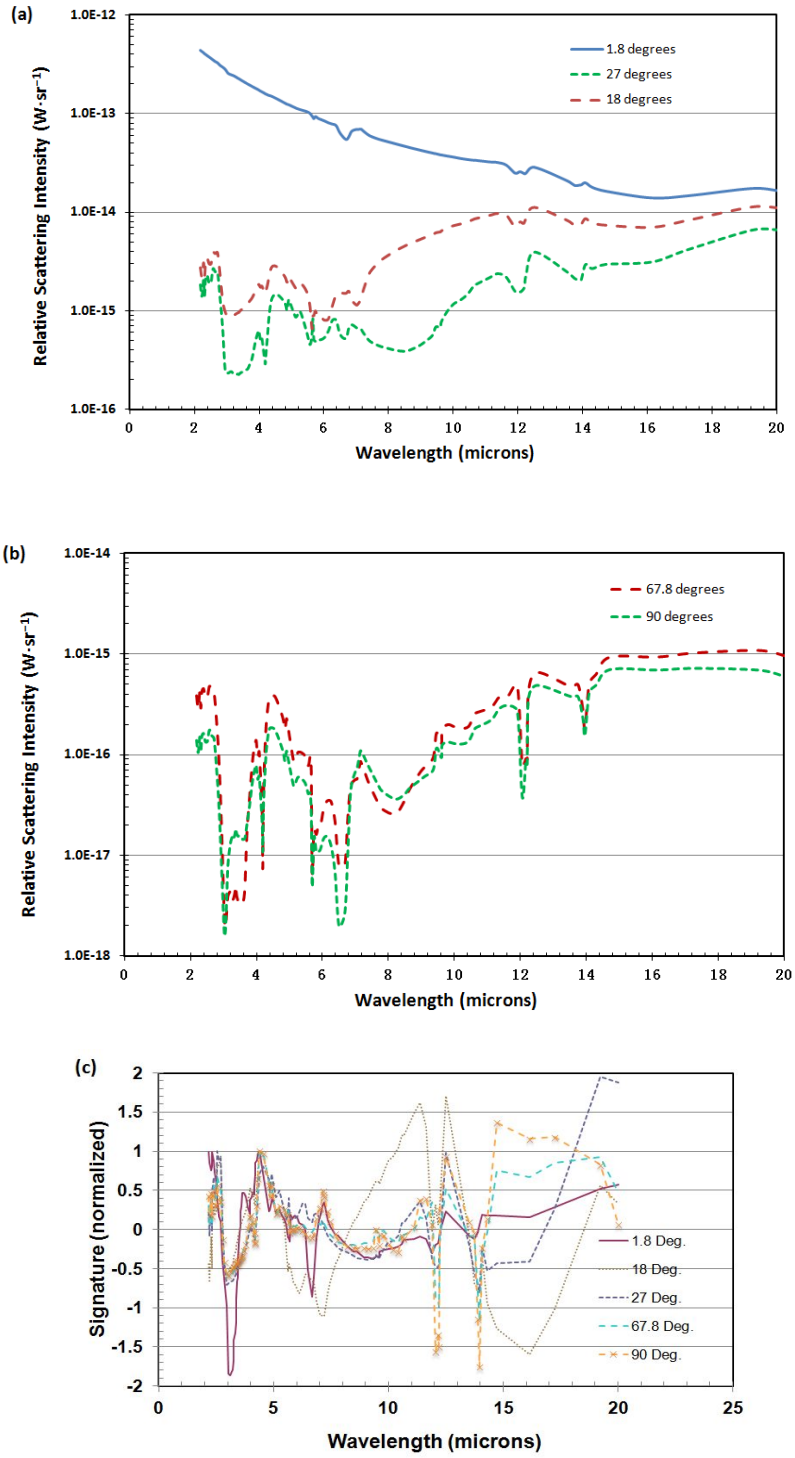

Figure 2. (a, b) The scattering radiant intensity of ammonium nitrate at large angles with CMD = 20 microns and $\sigma_g = 1.2$, assuming the incident light is parallel with the scattering plane, and (c) the corresponding spectral fingerprints.

To calculate the signatures, we remove the background by subtracting a best-fit third order polynomial from the data using the 'detrend' function in the freely available Octave environment. We then scale so that a large deviation from zero has unit magnitude. All signatures have a good response at small wavelengths, but the response is much stronger for the 1.8 degree data. The stronger weighting at smaller wavelengths of the aureole function is due to the strong scattering change with wavelength (and normalization). The spectral signature is shown on a linear scale. Larger angles contain features of similar size as the material-dependent features, and also these Mie resonances are also observed to change the magnitude of the material-dependent response at the signature wavelengths. Thus the signatures at 1.8 degree act as a better fingerprint.

3.2 Material dependence

The material dependent behavior is illustrated by the scattering intensity calculations shown in Figs. 3 and 4, which follow the complex index structure quite well. These calculations are made to simulate using a typical particle distribution: CMD = 10 micron and σ_g = 1.3. All have larger scattering power at small angles, and a decrease with wavelength that shows no sharp features besides those in the refractive indices. This background can be removed by filtering the low frequencies to obtain the spectral fingerprint. These data also point to the importance of examining a broad wavelength range when using this technique. Enough peaks in the fingerprint must be present to allow different species to be distinguished.

3.3 Concentration independence

Since we are attempting to identify the composition without regard to the particle characteristics, it is useful to demonstrate that concentration effects will not influence the result. Figure 4 shows the scattering calculation in comparison to the indices for two different concentrations of sulfuric acid. These data were simulated using the same typical particle distribution: CMD=10 micron and σ_g=1.3. The indices used here were obtained from experimental data. We could also have used effective medium theory to predict each from the concentrated sulfuric acid indices.

Figure 5 shows that the spectral fingerprint will be nearly independent of concentration of the chemical species. The strength of the scattering depends upon the concentration, but the location and relative strength of the features remains fixed. Since the spectral fingerprints will be normalized prior to comparison with experimental data, the two datasets would show the same identification as sulfuric acid. The concentration independence is more evident in the spectral fingerprints themselves. We show the spectral fingerprint from the scattering calculations in Fig. 4. These are calculated by detrending as above, then scaling so that the largest deviation from zero has unit magnitude. The results for the two different concentrations are shown in Fig. 5. The enhanced features on the spectral signature are much more readily visible without the background, and the normalization helps to make the signature nearly the same for these different concentrations.

3.4 Size independence

The final characteristic of the technique that we wish to demonstrate is the independence from particle size. Figure 6 shows the scattering calculation for several different particle size distributions within the aureole, at 1.8 degrees.

The calculation shows that for a wide range of particle distributions, when varying both the peak size from 5-20 μm and the width of the distribution, σ_g, all of the features that would become part of a normalized spectral fingerprint are preserved. In particular, although the scattering intensity is found to scale with the particle size, and the strength of the features depends upon both particle size and (more weakly) the distribution width, these spectral features remain the same. This is what is required for a robust fingerprint, so these data indicate the practicality of the proposed technique. The spectral fingerprints calculated as noted above are shown in Figure 7. The excellent agreement for smaller wavelengths is such that the different signatures can hardly be identified from one another. There is some deviation at larger wavelengths that is likely due to the simple 3rd order polynomial de-trending. The signatures are expected to be in better agreement with an optimal de-trending technique. Some difference for the smaller particles result from the larger relative influence of air scattering in the case of the smaller particles compared to the larger particles. We did not change the density of the particles to account for less scattering by smaller particles.

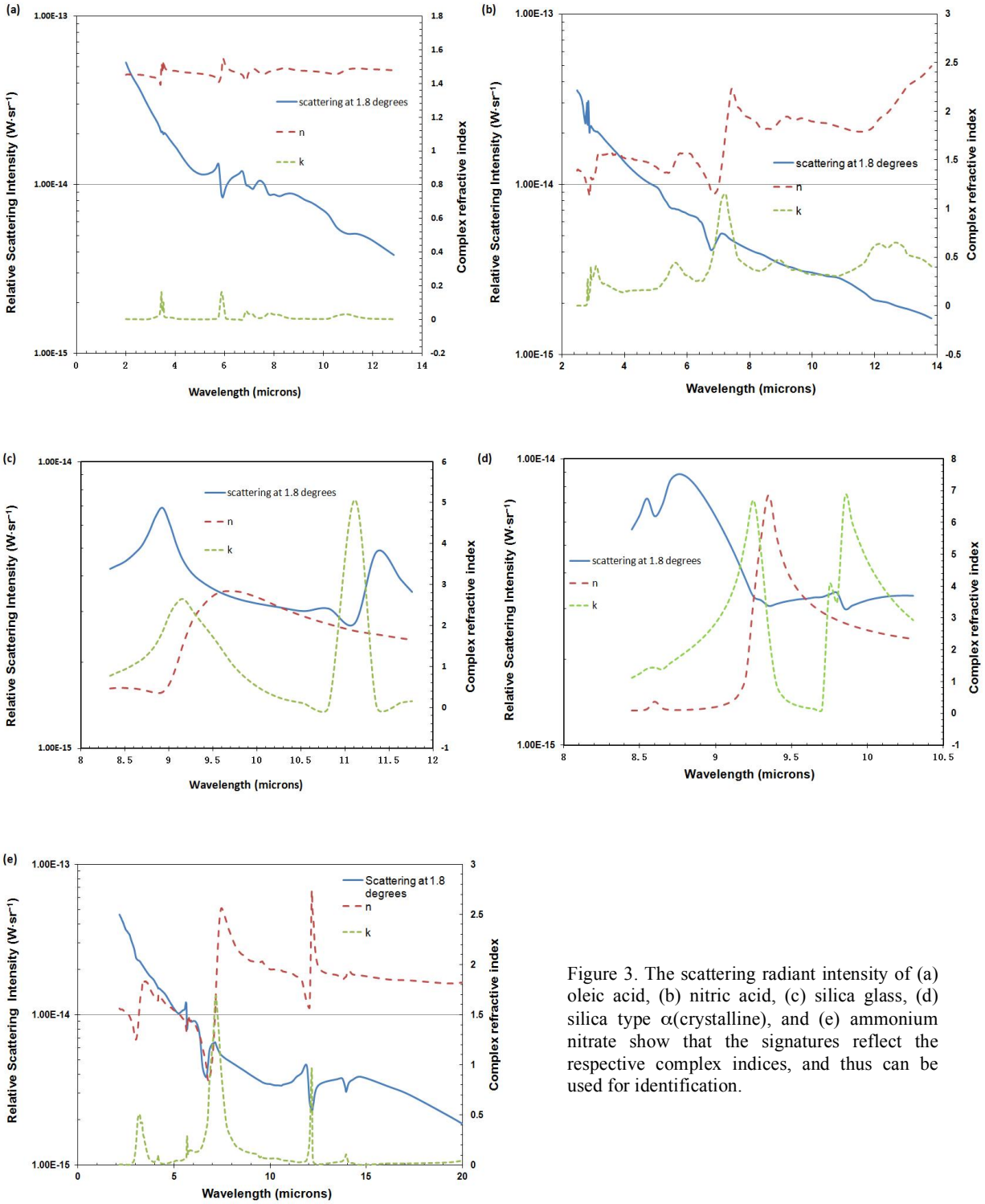

Figure 3. The scattering radiant intensity of (a) oleic acid, (b) nitric acid, (c) silica glass, (d) silica type α(crystalline), and (e) ammonium nitrate show that the signatures reflect the respective complex indices, and thus can be used for identification.

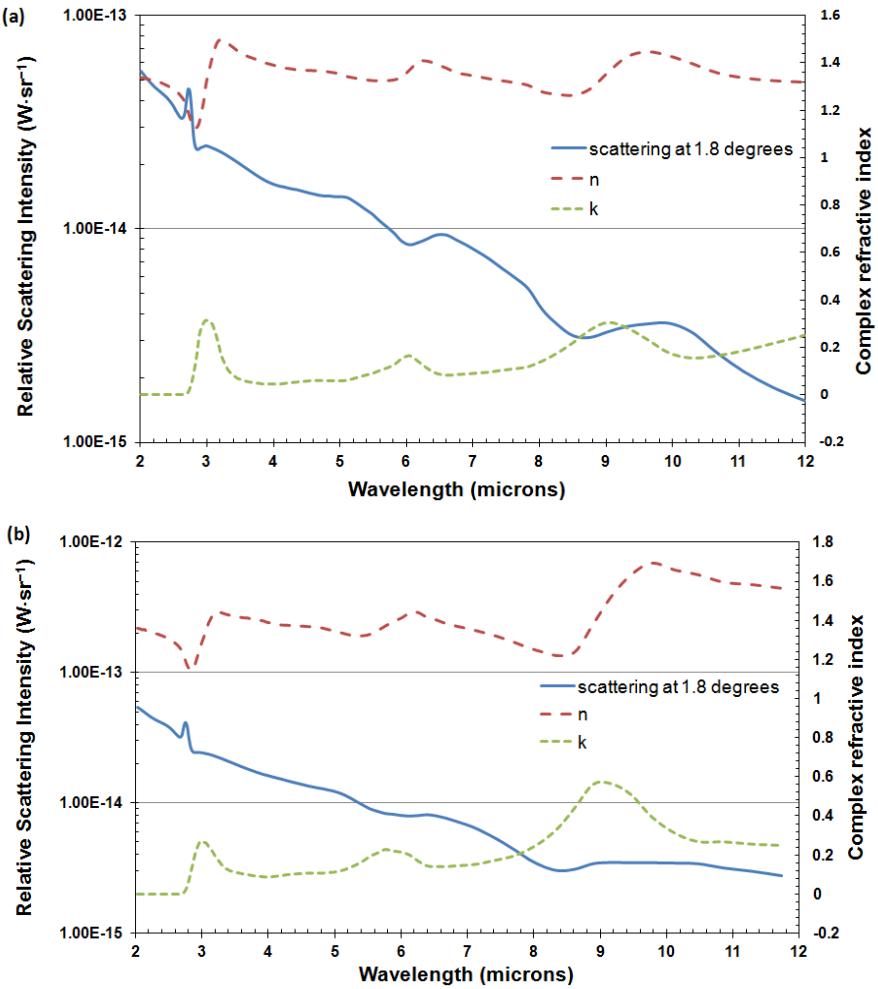

Figure 4. The scattering radiant intensity of sulfuric acid with concentrations of (a) 20 wt% and (b) 37 wt% show that the signatures for the same material are almost independent of concentration, since the magnitudes of the spectral fingerprints will be scaled to unity magnitude (particle properties are CMD = 10 micron and $\sigma_g = 1.3$).

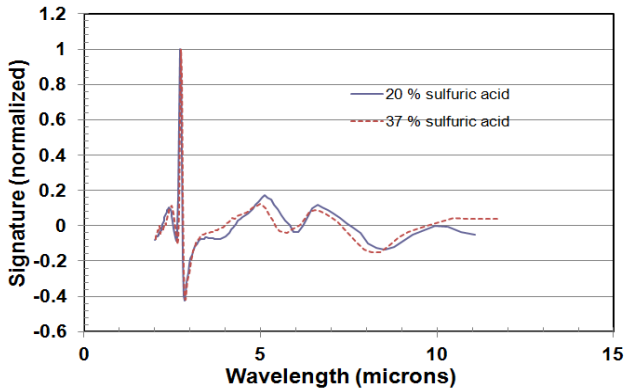

Figure 5. The spectral fingerprints of sulfuric acid with concentrations of 20% and 37% are almost the same (particle properties, CMD = 10 micron and $\sigma_g = 1.3$).

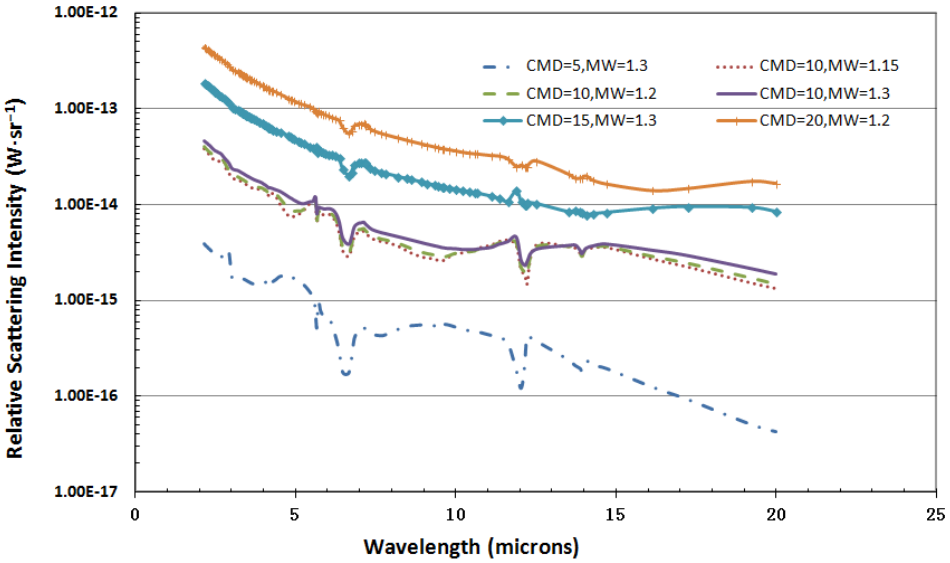

Figure 6. The scattering radiant intensity of ammonium nitrate with different size distributions.

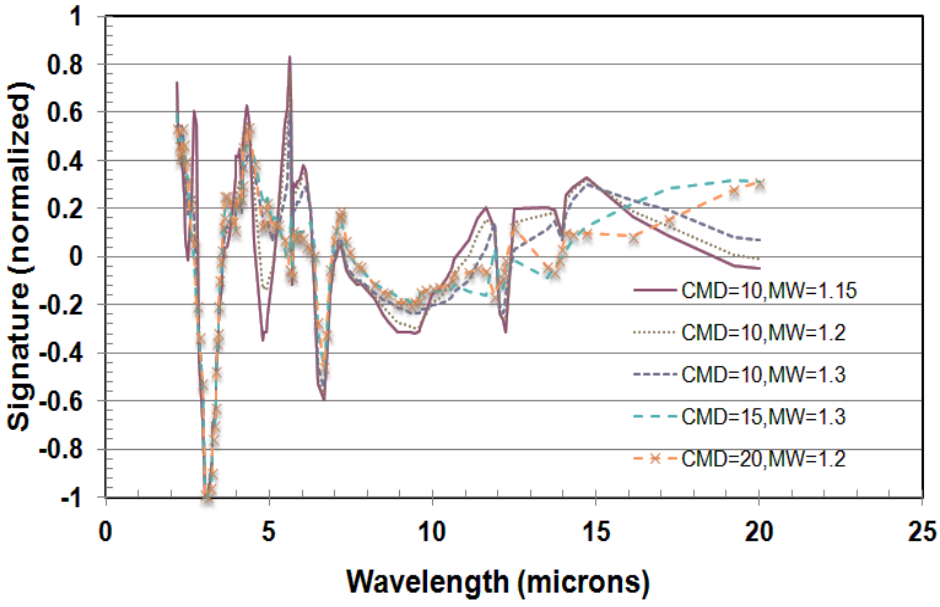

Figure 7. The spectral signature of ammonium nitrate with different size distributions.

3.5 Effective medium theory

From these scattering calculations, we could see that the scattering radiant intensity of these materials exhibits a signal that correlates well with their refractive index at the same wavelength and most of the minimums of scattering intensity coincide with the peaks of the imaginary refractive index k at the same wavelength. Some features exhibit small shifts between the scattering intensity and the refractive index, but these can be explained by effective medium theory. Because the aerosols are suspended in air, the dielectric properties, and therefore the real and imaginary indices of the

aerosols, are perturbed by screening charges that accumulate at the interfaces between the aerosols and the surrounding air molecules. Effective medium theories are used to describe these effects.

For isolated or sparsely dispersed (<5%) spheres in a host material (air in this case), the resulting effective complex dielectric constant can be found using the Maxwell-Garnett Equation,

$$\frac{\varepsilon - \varepsilon_h}{\varepsilon + 2\varepsilon_h} = f \frac{\varepsilon_b - \varepsilon_h}{\varepsilon_b + 2\varepsilon_h}, \quad (1)$$

where ε is the effective complex dielectric constant, ε_h is the complex dielectric constant of the host matrix, ε_b is the complex dielectric constant of the spherical inclusions, and f is the volume fraction of inclusions in the host material [37]. This effect is included in Mie calculations, since the Mie solution properly accounts for the surface boundary conditions [38]. This explains the deviation in some of our results.

If the scattering is from a complex combination of materials mixed into particles that are small compared to the wavelength of light used, then effective medium theory must be used to analyze the results. In this case, the spectral fingerprint to be extracted results from the effective index of the two materials combined. The dielectric surroundings for each molecule reflect the combination of shielding (induced dipole) of both species intermixed. The best effective medium theory to use is probably the Bruggeman [35]. This formulation uses the relationship,

$$0 = f_a \frac{\varepsilon_a - \varepsilon}{\varepsilon_a + 2\varepsilon} + f_b \frac{\varepsilon_b - \varepsilon}{\varepsilon_b + 2\varepsilon} + \ldots, \quad (2)$$

where ε is the effective complex dielectric constant, ε_a is the complex dielectric constant of material a, ε_b is the complex dielectric constant of material b, and f_a is the volume fraction of material a, and the sum of the volume fractions is 1. For two components, $f_b = 1 - f_a$. Although mixing substances will in general shift the sharp spectral features of the component's dielectric constants, inversion to the constituents and volume fractions should be possible in most few-component systems, if a sufficient wavelength range is used.

Such an accurate analysis of the features is not required for source identification applications, as that only requires correlation of the spectral fingerprints of the measured aerosols against source references.

4. CONCLUSIONS

The index of refraction of the materials that compose aerosols are wavelength-dependent. In particular, there are characteristic, sharp spectral features at particular, material-dependent, wavelengths. These features determine a material's spectral fingerprint, which will cause scattering calculations in the material to have 'high frequency' features at those wavelengths. These can be isolated, by removal of low frequency components and normalizing, to provide a spectral fingerprint, which can be used to identify the composition of the aerosols. We have shown calculations that predict measurements of the scattering intensity expected within the aureole region, which occurs near forward scattering. These calculations predict a large signal that is independent of particle shape or size (after removal of low frequency background). Density variations change the magnitude of the signal, but not the spectral fingerprint. The technique does not require assumptions about the particle size distribution or extensive measurements to identify it in addition to extracting the particle refractive index from the scattering data; thus, this approach makes analysis easier. The method does require measurements over a large wavelength range when the samples are completely unknown. It can be used for remote detection-in a real time system, with speed limited primarily by signal strength, path resolution, geometry, and detectors. Effective medium theory analysis will be required to identify complex mixtures of materials.

REFERENCES

[1] Pöschl, U., "Atmospheric Aerosols: Composition, Transformation, Climate and Health Effects," Angew. Chem. Int. Ed. 44, 7520-7540 (2005).

[2] Alfarra, M., [Insights into atmospheric organic aerosols using an aerosol mass spectrometer], PhD dissertation, The University of Manchester, UK (2004).

[3] Finlayson-Pitts, B. J., and J. N. Pitts Jr. [Chemistry of the upper and lower atmosphere: theory, experiments, and applications], Academic Press, San Diego, CA (2000).
[4] Chow, J. C. "Measurement methods to determine compliance with ambient air quality standards for suspended particles." Journal of the Air & Waste Management Association 45.5, 320-382 (1995).
[5] Spurny, K. R., ed. [Analytical Chemistry of Aerosols: Science and Technology], CRC Press, Boca Raton, FL (1999).
[6] McMurry, P. H. "A review of atmospheric aerosol measurements," Atmos. Environ. 34.12, 1959-1999 (2000).
[7] Jacobson, M. C., et al. "Organic atmospheric aerosols: Review and state of the science," Rev. Geophys. 38.2, 267-294 (2000).
[8] Kandler, K., et al. "Chemical composition and complex refractive index of Saharan Mineral Dust at Izana, Tenerife (Spain) derived by electron microscopy," Atmos. Environ. 41.37, 8058-8074 (2007).
[9] Ebert, M., S. Weinbruch, P. Hoffmann, and H. M. Ortner. "The chemical composition and complex refractive index of rural and urban influenced aerosols determined by individual particle analysis," Atmos. Environ. 38.38, 6531-6545 (2004).
[10] Jayne, J. T., et al. "Development of an aerosol mass spectrometer for size and composition analysis of submicro particles," Aerosol. Sci. Tech. 33.1-2, 49-70 (2000).
[11] Noble, Christopher A., and Kimberly A. Prather, "Real-time single particle mass spectrometry: A historical review of a quarter century of the chemical analysis of aerosols," Mass Spectrom. Rev. 19.4, 248-274 (2000).
[12] Gard, E., et al., "Real-time analysis of individual atmospheric aerosol particles: Design and performance of a portable ATOFMS," Anal. Chem. 69.20, 4083-4091 (1997).
[13] Van Wuijckhuijse, A. L., et al., "Matrix-assisted laser desorption/ionisation aerosol time-of-flight mass spectrometry for the analysis of bioaerosols: development of a fast detector for airborne biological pathogens," J. Aerosol. Sci.36.5, 677-687 (2005).
[14] Hansen, A. D. A., H. Rosen, and T. Novakov, "The aethalometer—an instrument for the real-time measurement of optical absorption by aerosol particles," Sci.Total.Environ. 36, 191-196 (1984).
[15] Huntzicker, J. J., R. S. Hoffman, and C.-S. Ling, "Continuous measurement and speciation of sulfur-containing aerosols by flame photometry," Atmos. Environ.(1967) 12.1, 83-88 (1978).
[16] Kittelson, D. B., et al. "Total sulfur aerosol concentration with an electrostatically pulsed flame photometric detector system." Atmos. Environ. 12.1, 105-111 (1978).
[17] Hinds, W. C. [Aerosol technology: properties, behavior, and measurement of airborne particles], John Wiley & Sons, New York (1999).
[18] Dubovik, O., et al., "Variability of absorption and optical properties of key aerosol types observed in worldwide locations," J. Atmos. Sci. 59.3 (2002).
[19] Tang, I. N., "Chemical and size effects of hygroscopic aerosols on light scattering coefficients," J. Geophys. Res. Atmos. (1984–2012) 101.D14, 19245-19250 (1996).
[20] Covert, D. S., R. J. Charlson, and N. C. Ahlquist. "A study of the relationship of chemical composition and humidity to light scattering by aerosols," J. Appl. Meteor. 11.6, 968-976 (1972).
[21] Deirmendjian, D., "Scattering and polarizaton properites of water clouds and hazes in the visible and infrared," Appl. Opt. 3.2, 187–196 (1964).
[22] Brown, A. M., Snyder, M. G., Brouwer, L., Philbrick, C. R., "Atmospheric aerosol characterization using multiwavelength multistatic light scattering," Proc. SPIE 7684, 76840I (2010).
[23] Philbrick, C. R., H. D. Hallen, A. M. Wyant, T. Wright, and M. Snyder, "Optical remote sensing techniques to characterize the properties of atmospheric aerosols," Proc. SPIE 7684, 76840J (2010).
[24] Hallen, H. D., B. J. Long, D. A. Hook, G. E. Pangle, C. R. Philbrick, "Multistatic lidar measurements of non-spherical aerosols," Proc SPIE 8731, 87310P (2013).
[25] Snyder, M., [Characterization of Aerosols Using Multiwavelength Multistatic Optical Scattering Data] PhD Dissertation, NC State University, Raleigh NC (2011).
[26] Bohren, C. F. and D. R. Huffman, D. R., [Absorption and scattering of light by small particles], Wiley, NewYork (1998).
[27] McGinty, S. M., M. K. Kapala, and R. F. Niedziela. "Mid-infrared complex refractive indices for oleic acid and optical properties of model oleic acid/water aerosols," Phys. Chem. Phys. 11.36, 7998-8004 (2009).
[28] Richwine, L.J., M. L. Clappa and R. E. Miller, "Complex refractive indices in the infrared of nitric acid trihydrate aerosols," Geophys. Res. Lett. 22, 2625-2628 (1995).

[29] Wagner, R., S. Benz, H. Bunz, O. Mohler, H. Saathoff,, M. Schnaiter, and T.Leisner, "Infrared Optical Constants of Highly Diluted Sulfuric Acid Solution Droplets at Cirrus Temperatures," J. Phys. Chem. A. 112, 11661-11676 (2008).
[30] Palik, E. D., ed. [Handbook of optical constants of solids] Academic Press, New York (1998).
[31] Jarzembski, M. A., et al. "Complex refractive index of ammonium nitrate in the 2–20-μm spectral range,"Appl. Opt., 42.6, 922-930 (2003).
[32] Wagner, R., et al., "A review of optical measurements at the aerosol and cloud chamber AIDA," J. Quant.Spectrosc. Ra. 110.11, 930-949 (2009).
[33] Ahrens, L. H., "The lognormal distribution of the elements (a fundamental law of geochemistry and its subsidiary)," Geochimica et Cosmochimica Acta 5.2, 49-73 (1954).
[34] Finlay, W. H., [The mechanics of inhaled pharmaceutical aerosols: an introduction], Academic Press, NewYork (2001).
[35] Brandon J.N. Long, D. A. Hook, Garret E. Pangle, Hans D. Hallen, C. Russell Philbrick, "Using a laser aureole to study aerosols," Proc. SPIE 8731, 87310O (2013).
[36] Liebsch, A., "Surface-plasmon dispersion and size dependence of Mie resonance: silver versus simple metals," Phys. Rev. B 48.15, 11317 (1993).
[37] Aspnes, D. E., J. B. Theeten, and F. Hottier, "Investigation of effective-medium models of microscopic surface roughness by spectroscopic ellipsometry," Phys. Rev. B 20.8 , 3292 (1979).
[38] D. A. Hook, G. E. Pangle, B. J.N. Long, C. R. Philbrick, and H. D. Hallen, "Understanding lidar returns from complex dust mixtures," Proc. SPIE 8731, 87310M (2013).